J. of Electromagn. Waves and Appl., Vol. 21, No. 9, 1231–1245, 2007

RADIATION FROM FIBONACCI-TYPE QUASIPERIODIC ARRAYS ON DIELECTRIC SUBSTRATES

G. Castaldi, V. Galdi, V. Pierro, and I. M. Pinto

Waves Group, Department of Engineering
University of Sannio
Corso Garibaldi 107, I-82100 Benevento, Italy

Abstract—We present a simple prototype study of electromagnetic radiation by a one-dimensional quasiperiodic Fibonacci-type array laid on a grounded dielectric slab, extending our previous free-space studies. Analytic parameterization of the interaction between aperiodic-order-induced "quasi-Floquet" waves and slab-induced surface/leaky-waves is addressed, for infinite and truncated arrays, via generalized Poisson summation and uniform asymptotics. Accuracy and computational effectiveness of the proposed parameterizations are assessed via numerical comparisons against an independently-generated reference solution (element-by-element synthesis).

1. INTRODUCTION AND PROBLEM FORMULATION

In a series of recent investigations [1–4], we studied the free-space radiation and scattering of electromagnetic (EM) waves by *aperiodically-ordered* structures. The interest in this type of geometries, intrinsically tied with the concept of "quasicrystals" in solid-state physics, is motivated by their growing relevance in many fields of science and technology (see [5] for a recent review on the subject, and [6] for an up-to-date bibliography database).

A major focus in our investigation is the *analytic parameterization* of aperiodic-order-induced wave phenomenologies, via extension and generalization of typical concepts and tools utilized in the study of *periodic* structures. In this framework, we studied in [2] the EM radiation from a class of one-dimensional (infinite and truncated) arrays based on Fibonacci-type sequences [7], which constitute one of the simplest paradigms of *quasiperiodic* order (see, e.g., [8] for an application to multilayer structures). Capitalizing on certain results from solid-state physics [7], we were able to derive a physically-insightful and computationally-effective parameterization of the radiated field in terms of "quasi-Floquet" (QF) waves, based on a *generalized Poisson summation formula*, thereby extending the studies carried out by Felsen and co-workers for strictly-periodic and weakly-aperiodic arrays (see, e.g., [9–11]) to a more general aperiodic scenario.

In this paper, we go one step further: Paralleling the study in [12], we address the analytic parameterization of the interaction between quasiperiodic-order-induced QF waves and the surface/leaky waves supported by a grounded dielectric slab. Referring to the geometry depicted in Fig. 1, we begin considering an infinite phased array of y-directed line sources placed at abscissas x_n on the surface $z = 0$ of a homogeneous dielectric slab of thickness b and relative permittivity ϵ_r, backed by a perfectly electric conducting (PEC) plane. The relevant current distribution, with implicit time-harmonic $\exp(j\omega t)$ excitation, is modeled by

$$J(x) = \sum_{n=-\infty}^{\infty} \delta(x - x_n) \exp\left(-j\eta k_0 x_n\right), \tag{1}$$

where $k_0 = \omega\sqrt{\epsilon_0\mu_0} = 2\pi/\lambda_0$ is the free-space wavenumber (with λ_0 being the wavelength), and $-1 \leq \eta \leq 1$ describes the inter-element phasing. As in [2], the element position sequence $\{x_n\}_{n=-\infty}^{\infty}$ is restricted to two possible inter-element spacings d_1 and $d_2 \leq d_1$ (see Fig. 1), and is chosen according to the modified-Fibonacci rule [7],

$$x_n = d_1 \left\| \frac{n}{\tau} \right\| + d_2 \left(n - \left\| \frac{n}{\tau} \right\| \right), \tag{2}$$

where $\|\cdot\|$ denotes the nearest-integer,

$$\|x\| = \begin{cases} n, & n \leq x < n + \frac{1}{2}, \\ n+1, & n + \frac{1}{2} \leq x \leq n+1, \end{cases} \tag{3}$$

and $\tau \equiv (1 + \sqrt{5})/2$ is the *Golden Mean*. The modified-Fibonacci sequence in (2) is a generally *quasiperiodic* sequence, which can also be generated via cut-and-project schemes or substitution rules (see [2, 7] and the references therein for more details as well as possible extensions/generalizations). Such sequence includes as special cases the *periodic* ($d_1 = d_2$) and standard Fibonacci ($d_2 = d_1/\tau$) cases.

Following [2], it is expedient to parameterize the sequence in (2) in terms of the average spacing d_{av} (in the infinite-sequence limit) [7]

$$d_{av} = \frac{\tau d_1 + d_2}{1 + \tau} \tag{4}$$

and the scale ratio $\nu = d_2/d_1$, expressing d_1 and d_2 as

$$d_1 = \frac{(1+\tau)}{(\nu+\tau)} d_{av}, \quad d_2 = \nu d_1, \quad 0 < \nu \leq 1. \tag{5}$$

Paralleling [12], the goal of this investigation is to study the radiated field distribution into the halfspace $z > 0$. Attention is restricted to the y-directed electric field $U(r, \theta)$, which can be expressed via element-by-element superposition as

$$U(r, \theta) = \sum_n U_n(R_n, \theta_n) \exp(-j\eta k_0 x_n). \tag{6}$$

In (6), which throughout the paper will be used as a reference solution, $U_n(R_n, \theta_n)$ denotes the field radiated by a nonphased line-source located at x_n (see Fig. 1) in the presence of the grounded dielectric slab (see Appendix A for a uniform asymptotic approximation), and the summation includes all the line-source elements. In what follows, starting from the background results in free space [2], an alternative parameterization will be presented, based on Poisson-summation-type concepts.

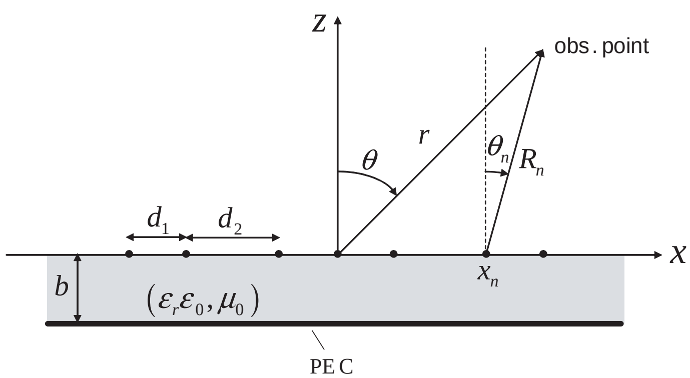

Figure 1. Problem schematic: An infinite (or semi-infinite) phased array of y-directed line sources is located on top of a PEC-backed dielectric slab with relative permittivity ϵ_r and thickness b. The element distribution x_n, which features only two possible inter-element spacings d_1 and $d_2 \leq d_1$, is chosen according to the modified-Fibonacci sequence in (2). Also shown are the global (r, θ) and local (R_n, θ_n) polar coordinate systems utilized.

2. BACKGROUND: FIBONACCI-TYPE ARRAYS IN FREE SPACE

In [2], based on certain results in [7], it was shown that the current distribution in (1) can be recast as

$$J(x) = \frac{1}{d_{av}} \sum_{q_1,q_2=-\infty}^{\infty} S_{q_1 q_2} \exp\left(-jk_{xq_1q_2} x\right), \tag{7}$$

where d_{av} is defined in (4), and the amplitude coefficients $S_{q_1q_2}$ and spatial frequencies $k_{xq_1q_2}$ are given by

$$S_{q_1q_2} = \frac{\sin W_{q_1q_2}}{W_{q_1q_2}}, \quad W_{q_1q_2} = \frac{\pi(1+\tau)(q_1 - q_2\nu)}{\nu+\tau}, \tag{8}$$

$$k_{xq_1q_2} = k_0\eta + \frac{2\pi}{d_{av}} \frac{(q_1 + q_2\tau)}{(\tau+1)}. \tag{9}$$

The main results and observations in [2], which represent the starting point for the present investigation, can be summarized as follows.

- Equation (7) represents a *generalized Poisson summation formula* (GPSF), which applies to the general quasiperiodic modified-Fibonacci array in (2), and reduces to the standard Poisson summation [13] for the special case of *periodic* arrays ($d_1 = d_2$, i.e., $\nu = 1$).
- The GPSF generally entails a (q_1, q_2)-indexed *double* infinity of *pairwise-incommensurate* spatial frequencies $k_{xq_1q_2}$ which depend only on the average inter-element spacing d_{av} and phasing $k_0\eta$. The scale-ratio ν affects (via $W_{q_1q_2}$) the amplitude coefficients $S_{q_1q_2}$ in (8). The spatial spectrum is periodic *if and only if* the scales d_1 and d_2 are commensurate.
- As for the periodic case (see, e.g., [9–11]), the GPSF can be exploited to efficiently parameterize the radiation by Fibonacci-type quasiperiodic arrays in free space. The degree of freedom in the choice of the scale-ratio ν can be exploited to control certain radiation characteristics (e.g., secondary beams).

3. FIBONACCI-TYPE ARRAYS ON DIELECTRIC SUBSTRATES

3.1. Infinite Arrays

In the presence of the PEC-backed dielectric slab, the y-polarized electric field radiated into the $z > 0$ halfspace by the quasiperiodic modified-Fibonacci current distribution $J(x)$ in (1) (or its GPSF-equivalent in (7)) can be synthesized via straightforward plane-wave representation in terms of the spectral integral [14, Sec. 5.6]

$$U(x,z) = -\frac{1}{2\pi}\int_{-\infty}^{\infty} \hat{J}(k_x)\hat{Z}(k_x)\exp\left[-j\left(k_x x + k_z z\right)\right] dk_x. \tag{10}$$

In (10), k_x and $k_z = \sqrt{k_0^2 - k_x^2}$, $\mathrm{Im}(k_z) \le 0$, are the x- and z-domain wavenumbers, respectively, and $\hat{J}(k_x)$ denotes the spatial Fourier transform (plane-wave spectrum) of $J(x)$, which, applying the GPSF in (7), yields

$$\hat{J}(k_x) = \int_{-\infty}^{\infty} J(x)\exp\left(jk_x x\right) dx = \frac{2\pi}{d_{av}} \sum_{q_1,q_2=-\infty}^{\infty} S_{q_1,q_2}\delta\left(k_x - k_{xq_1q_2}\right). \tag{11}$$

Here and henceforth, the caret ˆ denotes plane-wave spectral quantities. Moreover, in (10), the spectral impedance

$$\hat{Z}(k_x) = \frac{j\omega\mu_0\tan\left(\sqrt{k_0^2\epsilon_r - k_x^2}b\right)}{\sqrt{k_0^2\epsilon_r - k_x^2} + jk_z\tan\left(\sqrt{k_0^2\epsilon_r - k_x^2}b\right)} \tag{12}$$

accounts for the slab-loading effects [14, Sec. 5.6]. Thanks to the Dirac-delta-comb structure of its integrand (cf. (11)), the spectral integral in (10) can readily be computed in closed form, yielding a QF plane-wave representation, which can be recast in the (r,θ) coordinate system (see Fig. 1) as

$$U(r,\theta) = \sum_{q_1,q_2=-\infty}^{\infty} S_{q_1q_2}U_{q_1q_2}^{QF}(r,\theta), \tag{13}$$

$$U_{q_1q_2}^{QF}(r,\theta) = -\frac{Z_p(\Theta_{q_1q_2})}{d_{av}}\exp\left[-jk_0 r\cos\left(\Theta_{q_1q_2} - \theta\right)\right]. \tag{14}$$

In (14), the spectral mapping $k_x = k_0\sin\Theta$ has been introduced, so that

$$Z_p(\Theta) = \hat{Z}(k_0\sin\Theta) \tag{15}$$

denotes the "pattern function" associated with the slab-loading, and

$$\Theta_{q_1q_2} = \arcsin\left(\frac{k_{xq_1q_2}}{k_0}\right), \quad \mathrm{Im}\left(\Theta_{q_1q_2}\right) \le 0 \tag{16}$$

denote the QF wave spectral directions related to the x-domain wavenumbers $k_{xq_1q_2}$ in (9). The electric field in (13) is thus synthesized in terms of *an infinity* of amplitude-modulated (via (15)) *propagating* ($|k_{xq_1q_2}| < k_0$) QF plane waves with arrival directions $\Theta_{q_1q_2}$, corresponding to the summation indexes (see [2] for details)

$$q_2 \lessgtr -\frac{q_1}{\tau} \pm \left(\frac{d_{av}}{\lambda_0}\right) \frac{(1 \mp \eta)(1+\tau)}{\tau}, \qquad (17)$$

plus an infinity of *evanescent* ($|k_{xq_1q_2}| > k_0$) QF plane waves. Evanescent QF waves yield negligible contributions at observation points far from the array plane. However, for *truncated* arrays (see below), they originate *propagating diffracted* fields that need to be taken into account.

3.2. Truncation Effects

As for the free-space case [2], radiation from the semi-infinite ($n \geq 0$) version of the array in (1) can be parameterized in terms of a *truncated* QF wave superposition,

$$\begin{aligned} U_T(r,\theta) &= \sum_{n=0}^{\infty} U_n(r,\theta) \exp(-j\eta k_0 x_n) \\ &= \frac{U_0(r,\theta)}{2} + \sum_{q_1,q_2=-\infty}^{\infty} S_{q_1q_2} U_{q_1q_2}^T(r,\theta), \end{aligned} \qquad (18)$$

by using the one-sided version of the GPSF (which generalizes the results in [13]). In (18), $U_0(r,\theta)$ is the electric field radiated by a line source located at $x = 0$ (see Appendix A for a uniform asymptotic approximation), whereas the expansion in terms of *truncated* QF wave propagators $U_{q_1q_2}^T$ stems from the spectral integral in (10) by considering, instead of the infinite-array current spectrum $\hat{J}(k_x)$ in (11), the *truncated-array* current spectrum

$$\hat{J}_T(k_x) = \int_0^{\infty} J(x) \exp(jk_x x)\, dx = \frac{j}{d_{av}} \sum_{q_1,q_2=-\infty}^{\infty} \frac{S_{q_1q_2}}{k_x - k_{xq_1q_2}}. \qquad (19)$$

Accordingly, the truncated QF propagators in (18) are synthesized as

$$U_{q_1q_2}^T(x,z) = \frac{1}{2\pi j d_{av}} \int_{-\infty}^{\infty} \frac{\hat{Z}(k_x)}{k_x - k_{xq_1q_2}} \exp\left[-j\left(k_x x + k_z z\right)\right] dk_x. \qquad (20)$$

It is expedient to rewrite the integrand in (20) by using

$$\frac{\hat{Z}(k_x)}{k_x - k_{xq_1q_2}} = \frac{\hat{Z}(k_{xq_1q_2})}{k_x - k_{xq_1q_2}} + \frac{\hat{Z}(k_x) - \hat{Z}(k_{xq_1q_2})}{k_x - k_{xq_1q_2}}, \tag{21}$$

so as to separate the singularities induced by quasiperiodicity (QF-wave pole at $k_x = k_{xq_1q_2}$, in the first term in the right hand side of (21)) from those induced by the slab-loading (branch-point at $k_x = k_0$ plus surface/leaky-wave poles [14, Sec. 5.6], in the second term in the right hand side of (21)). By introducing the canonical complex-plane mapping $k_x = k_0 \sin\Theta$ (which eliminates the branch-point singularity [14, Sec. 5.6]), and for large observation distance ($k_0 r \gg 1$), the two arising integrals can be approximated via uniform saddle-point asymptotics (first-order saddle-point nearby a simple† pole singularity [14, Sec. 4.4a]), yielding

$$U^T_{q_1q_2}(r,\theta) = F_{q_1q_2}(r,\theta) + G_{q_1q_2}(r,\theta). \tag{22}$$

The first term on the right hand side of (22) arises from the QF-wave pole at $k_x = k_{xq_1q_2}$, and is given by

$$\begin{aligned} F_{q_1q_2}(r,\theta) \quad &\sim \quad \frac{Z_p(\Theta_{q_1q_2})}{2\pi j d_{av}} \exp\left[-jk_0 r \cos(\Theta_{q_1q_2} - \theta)\right] \\ &\times \quad \left[\sqrt{\frac{2\pi}{k_0 r}} \exp(j\pi/4) \frac{\cos\theta - \cos\left(\frac{\theta + \Theta_{q_1q_2}}{2}\right)}{\sin\theta - \sin\Theta_{q_1q_2}} \right. \\ &\pm \quad 2j\sqrt{\pi} \exp\left(-k_0 r \beta^2_{q_1q_2}\right) Q\left(\mp j\beta_{q_1q_2}\sqrt{k_0 r}\right) \\ &- \quad \left. 2j\pi H\left(\theta - \Theta^{SB}_{q_1q_2}\right) \right], \quad \mathrm{Im}\left(\beta_{q_1q_2}\right) \gtrless 0, \end{aligned} \tag{23}$$

where $H(\cdot)$ is the Heaviside unit-step function,

$$Q(\xi) = \sqrt{\pi} - Q(-\xi) = \int_{\xi}^{\infty} \exp(-\zeta^2) d\zeta \tag{24}$$

is the error function complement [15], and

$$\beta_{q_1q_2} = \sqrt{2} \exp(-j\pi/4) \sin\left(\frac{\Theta_{q_1q_2} - \theta}{2}\right). \tag{25}$$

† We restrict our attention to the simplest and most common case where QF-wave and surface-wave poles are *distinct*. Otherwise, the corresponding asymptotic approximations for *double* poles [14, Sec. 4.4b] need to be applied.

Equation (23) represents a truncated propagator with arrival spectral direction $\Theta_{q_1q_2}$ in (16), and excitation amplitude modulated by the slab-loading pattern-function in (15), limited by a conical shadow boundary at

$$\Theta^{SB}_{q_1q_2} = \mathrm{Re}\left(\Theta_{q_1q_2}\right) - \mathrm{sign}\left[\mathrm{Im}\left(\Theta_{q_1q_2}\right)\right] \arccos\left\{\frac{1}{\cosh\left[\mathrm{Im}\left(\Theta_{q_1q_2}\right)\right]}\right\}, \tag{26}$$

which corresponds to the observation direction for which the steepest-descent path in the complex Θ-plane crosses the QF-wave complex pole at $\Theta_{q_1q_2}$. The second term on the right hand side of (22), which accounts for the slab-induced surface/leaky-wave contributions excited by the (q_1, q_2)-indexed QF wave, is given by

$$\begin{aligned} G_{q_1q_2}(r,\theta) \sim \frac{1}{2\pi j d_{av}} \sum_m & \exp\left[-jk_0 r \cos\left(\Theta_m - \theta\right)\right] \\ \times\Bigg\{ & \sqrt{\frac{\pi}{k_0 r}} \frac{\alpha^{(m)}_{q_1q_2}}{\beta_m} + \sqrt{\frac{2\pi}{k_0 r}} \Lambda_{q_1q_2}\left(\Theta_m\right) \cos\Theta_m \ \exp\left(j\frac{\pi}{4}\right) \\ & \pm j2\pi\alpha^{(m)}_{q_1q_2} \cos\Theta_m H\big[\theta\ \Theta^{SB}_{q_1q_2}\big]\ H\big[|\theta| - \big|\Theta^{SB}_{q_1q_2}\big|\big] \\ & \pm 2\sqrt{\pi} j \alpha^{(m)}_{q_1q_2} Q\left(\mp j\beta_m\right) \exp\left(-k_0 r \beta^2_m\right)\Bigg\}, \quad \mathrm{Im}(\beta_m) \gtrless 0. \end{aligned} \tag{27}$$

In (27), the m-summation includes the dominant surface/leaky-wave poles Θ_m of the function

$$\Lambda_{q_1q_2}(\Theta) = \frac{Z_p(\Theta) - Z_p(\Theta_{q_1q_2})}{\sin\Theta - \sin\Theta_{q_1q_2}} \tag{28}$$

in the complex Θ-plane captured during the deformation of the original Sommerfeld path into the steepest-descent path (SDP) through the saddle point $\Theta_s = \theta$ (see [14, Sec. 4.4a] for details), $\alpha^{(m)}_{q_1q_2}$ denote the corresponding (counterclockwise) residues, and

$$\beta_m = \sqrt{2}\exp(-j\pi/4)\sin\left(\frac{\Theta_m - \theta}{2}\right). \tag{29}$$

The above semi-infinite array QF synthesis can readily be adapted to the case of *finite* arrays by expressing the array interval as the difference between two overlapping semi-infinite intervals.

4. REPRESENTATIVE RESULTS

We now move on to illustrating some representative results, based on the comparison between the proposed truncated QF synthesis in (18) and the reference solution (element-by-element synthesis, cf. (6) and Appendix A). Both solutions are numerically implemented by retaining $M = 10$ dominant surface/leaky-wave poles, computed via numerical (Newton-Raphson) solution of the non-linear dispersion equation pertaining to the PEC-backed dielectric slab, exploiting as initial guesses the low-frequency approximations in [16].

We begin considering a 101-element nonphased standard-Fibonacci array ($\eta = 0$, $\nu = 1/\tau$, $|n| \leq 50$ in (1)) with $d_{av} = 0.5\lambda_0$, located on top of a PEC-backed dielectric slab with low relative permittivity $\epsilon_r = 1.1$ and thickness $b = \lambda_0/(8\sqrt{\epsilon_r})$. Figure 2 compares two truncated QF syntheses in the array *near-zone* ($r = 100\lambda_0$), obtained retaining $N_p = 3$ and $N_p = 9$ propagating QF waves in (18), and the reference solution in (6) (with $|n| \leq 50$). It is observed that a few dominant propagating QF waves are sufficient to capture the essential features of the wavefield structure. Similar observations hold for the far-field pattern in Fig. 3. As in [2], to better quantify the

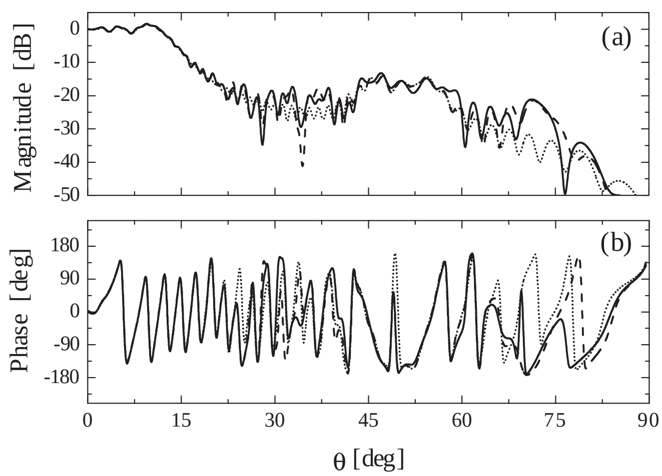

Figure 2. 101-element Fibonacci-type array with $d_{av} = 0.5\lambda_0$, $\nu = 1/\tau$, and $\eta = 0$. Near-zone ($r = 100\lambda_0$) normalized field scan. QF syntheses retaining $N_p = 3$ and $N_p = 9$ dominant propagating waves (selected within $|q_1|, |q_2| \leq 50$) are displayed as dotted and dashed curves, respectively. Reference solution (element-by-element summation) is displayed as a continuous curve. Due to symmetry, only positive angles are shown.

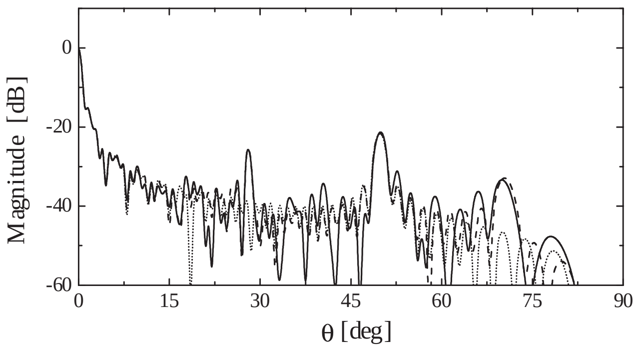

Figure 3. As in Fig. 2, but far-field pattern.

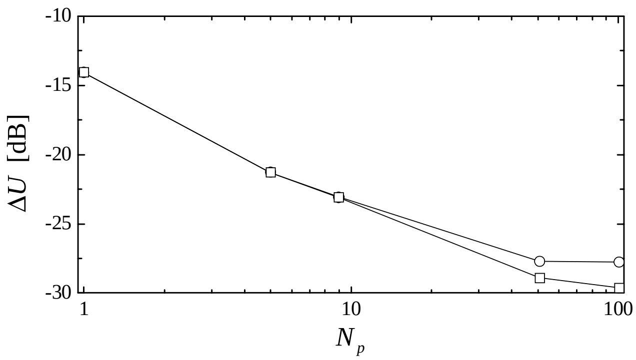

Figure 4. Parameters as in Fig. 2, but r.m.s. error ΔU in (30) as a function of the number N_p of propagating waves retained in the near-zone ($r = 100\lambda_0$) QF synthesis. Circular bullets: No evanescent waves retained. Square bullets: $N_e = N_p$ evanescent waves retained.

accuracy and address convergence issues, we have computed the r.m.s. error

$$\Delta U(r) = \sqrt{\frac{\int_{-\pi/2}^{\pi/2} \left|U^{RS}(r,\theta) - U^{QF}(r,\theta)\right|^2 d\theta}{\int_{-\pi/2}^{\pi/2} \left|U^{RS}(r,\theta)\right|^2 d\theta}}, \tag{30}$$

where the superscripts "^{RS}" and "^{QF}" denote the reference solution and the QF synthesis, respectively. The r.m.s. error behavior, for the near-zone synthesis of Fig. 2, is shown in Fig. 4 as a function of the number N_p of dominant propagating QF waves retained, and also compared with that obtained by retaining a number $N_e = N_p$

of dominant evanescent QF diffracted waves. As for the free-space case [2], it is observed that acceptable accuracies ($\Delta U \sim -20\,\mathrm{dB}$) are obtained by retaining a small number (~ 10) of QF waves, with the evanescent diffracted waves yielding visible improvements only at larger N_e-values. Results for the far-field are practically identical.

A thorough parametric analysis has been carried out in order to validate and calibrate the proposed QF wave synthesis. As an example, Fig. 5 shows the r.m.s. error behavior for various values of the slab relative permittivity ϵ_r and thickness b. The consistently poorer accuracy observed for half-wavelength-thick slabs (triangular bullets in Fig. 5) is intuitively attributable to the weak radiation caused by the low-impedance (short-circuit at broadside) loading.

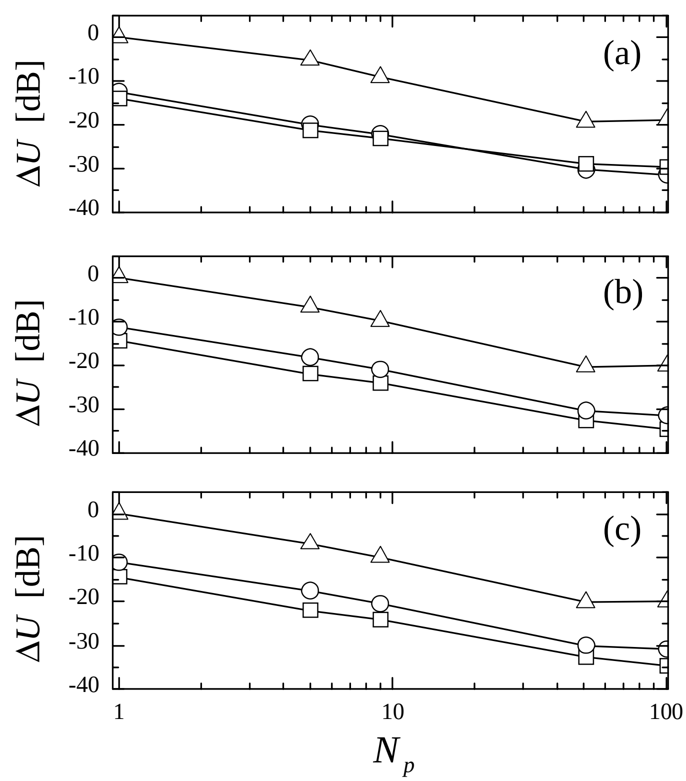

Figure 5. As in Fig. 4, with $N_e = N_p$, and various values of the slab relative permittivity ϵ_r and thickness b. (a), (b), (c): $\epsilon_r = 1.1, 5, 10$, respectively. Square, circular, triangular bullets: $b = \lambda_0/(8\sqrt{\epsilon_r}), \lambda_0/(4\sqrt{\epsilon_r}), \lambda_0/(2\sqrt{\epsilon_r})$, respectively.

Similar results, not shown here for brevity, have been observed for different inter-element spacing, scale-ratio, phasing, (moderate to large) array sizes and observation distances. As for the free-space case [2], one observes a faster convergence in the presence of weaker aperiodicity ($\nu \approx 1$) and smaller average inter-element spacings, and viceversa.

5. CONCLUSIONS

In this paper, as a further step in our ongoing research agenda focused on wave interactions with aperiodic order, we have presented a simple prototype study involving a quasiperiodic Fibonacci-type 1-D array radiating in the presence of a PEC-backed dielectric slab. In this connection, the QF analytic parameterizations derived for infinite and semi-infinite Fibonacci-type arrays in free space [2], based on a GPSF, have been extended here to account for the interaction between quasiperiodicity-induced QF waves and slab-induced surface/leaky-waves, via uniform asymptotic approximation of the arising spectral integrals. Numerical results have been presented in order to validate and calibrate the proposed parameterizations, confirming their accuracy and computational effectiveness in this more complicated scenario.

Current and future investigations are aimed at the exploration of antenna arrays based on other aperiodic arrangements (e.g., Thue-Morse, period-doubling, Rudin-Shapiro [4]), as well as the exploitation of the additional degrees of freedom available in aperiodic structures in applications to array radiation pattern control, radar signatures, radio-frequency identification, frequency selective surfaces, etc. In this connection, also of interest is the study of aperiodic arrays on metamaterial slabs [17, 18] for applications to gratings [19] and microstrip antennas [20].

ACKNOWLEDGMENT

This paper is dedicated to the dear memory of Professor Leo Felsen, mentor and friend. Professor Felsen posed the problem discussed in this paper, and provided unvaluable suggestions at the early stage of this research project.

APPENDIX A. LINE-SOURCE RADIATION IN THE PRESENCE OF A DIELECTRIC SLAB

The y-directed electric field radiated by a unit-amplitude (nonphased) line-source located on top of a PEC-backed dielectric slab at $x = x_n$ (see Fig. 1) at the observation point (x, z), in the local polar coordinate system ($R_n \equiv \sqrt{(x-x_n)^2 + z^2}, \theta_n \equiv \arcsin[(x-x_n)/R_n]$), can be parameterized asymptotically ($k_0 R_n \gg 1$) as [14, Sec. 5.6]

$$U_n(R_n, \theta_n) \sim U_{SW_n}(R_n, \theta_n) + U_{LW_n}(R_n, \theta_n), \tag{A1}$$

where U_{SW_n} and U_{LW_n} represent the space-wave and surface/leaky-wave contributions, respectively. Assuming that the phase of the slab-loading pattern-function $Z_p(\theta_n)$ in (15) varies slowly[‡] with respect to $\exp(-jk_0 R_n \cos\theta_n)$, with the canonical complex mapping $k_x = k_0 \sin\Theta$, one obtains via saddle-point uniform asymptotics [14, Sec. 5.6]

$$U_{SW_n}(R_n, \theta_n) = -\sqrt{\frac{k_0}{2\pi R_n}} Z_p(\theta_n) \cos\theta_n \exp\left[-j\left(k_0 R_n - \pi/4\right)\right], \tag{A2}$$

$$U_{LW_n}(R_n, \theta_n) = \sum_m \left[L_m(R_n, \theta_n, \Theta_m) + D_m(R_n, \theta_n, \Theta_m)\right], \tag{A3}$$

where

$$L_m(R_n, \theta_n, \Theta_m) = \pm 2\pi j \alpha_m \cos\Theta_m \exp[-jk_0 R_n \cos(\Theta_m - \theta_n)] \times H\left[|\theta_n| - |\Theta_m^{SB}|\right] H\left[\theta_n\ \Theta_m^{SB}\right],\ \Theta_m^{SB} \lessgtr 0, \tag{A4}$$

$$D_m(R_n, \theta_n, \Theta_m) \sim \pm 2\sqrt{\pi} j \alpha_m Q(\mp j\beta_m) \exp(-k_0 R_n \beta_m^2),\ \mathrm{Im}(\beta_m) \gtrless 0. \tag{A5}$$

The space-wave contribution U_{SW_n} in (A2) corresponds to a free-space outgoing cylindrical wave centered at x_n, modulated by the slab-loading factor $Z_p(\theta_n)$ in (15). The m-summation in (A3) includes the dominant surface/leaky-wave poles Θ_m in the complex Θ-plane captured during the deformation of the original Sommerfeld path into the SDP through the saddle point $\Theta_s = \theta_n$ (see [14, Sec. 4.4a] for details). In (A4), α_m is the (counterclockwise) residue in Θ_m of the slab-loading pattern-function $Z_p(\Theta)$ in (15). The surface/leaky-wave term L_m in (A4), with excitation amplitude α_m, represents a truncated plane-wave contribution (evanescent in the case of surface

‡ Otherwise Z_p needs to be decomposed into multiple reflected wave terms inside the slab, with separate asymptotic treatment for those refraction contributions into free space with rapidly-varying phases [14, Sec. 4].

wave) at the complex angle Θ_m, limited by a conical shadow boundary at Θ_m^{SB} (given in (26), with Θ_m replacing $\Theta_{q_1 q_2}$). The wavefield continuity across the parabolic transition region surrounding the shadow boundary is ensured by the diffraction term D_m in (A5), with $Q(\cdot)$ denoting the error function complement in (24), and β_m given in (29).

REFERENCES

1. Pierro, V., V. Galdi, G. Castaldi, I. M. Pinto, and L. B. Felsen, "Radiation properties of planar antenna arrays based on certain categories of aperiodic tilings," *IEEE Trans. Antennas Propagat.*, Vol. 53, 635–644, 2005.
2. Galdi, V., G. Castaldi, V. Pierro, I. M. Pinto, and L. B. Felsen, "Parameterizing quasiperiodicity: Generalized Poisson summation and its application to modified-Fibonacci antenna arrays," *IEEE Trans. Antennas Propagat.*, Vol. 53, 2044–2053, 2005.
3. Galdi, V., V. Pierro, G. Castaldi, I. M. Pinto, and L. B. Felsen, "Radiation properties of one-dimensional random-like antenna arrays based on Rudin-Shapiro sequences," *IEEE Trans. Antennas Propagat.*, Vol. 53, 3568–3575, 2005.
4. Galdi, V., G. Castaldi, V. Pierro, I. M. Pinto, and L. B. Felsen, "Scattering properties of one-dimensional aperiodically-ordered strip arrays based on two-symbol substitutional sequences," *IEEE Trans. Antennas Propagat. (Special Issue on "Electromagnetic Wave Propagation in Complex Environments: A Tribute to Leopold Benno Felsen")*, Vol. 54, 2007 (in print).
5. Maciá, E., "The role of aperiodic order in science and technology," *Rep. Progr. Phys.*, Vol. 69, 397–441, 2006.
6. http://www.quasi.iastate.edu/bib.html, maintained by the Quasicrystal Research Group at Iowa State University, IA, USA.
7. Buczek, P., L. Sadun, and J. Wolny, "Periodic diffraction patterns for 1D quasicrystals," *Acta Physica Polonica B*, Vol 36, 919–933, 2005.
8. Aissauoi, M., J. Zaghdoudi, M. Kanzari, and B. Rezig, "Optical properties of the quasi-periodic one-dimensional generalized multilayer Fibonacci structures," *Progress In Electromagnetics Research*, PIER 59, 69–83, 2006.
9. Carin L. and L. B. Felsen, "Time-harmonic and transient scattering by finite periodic flat strip arrays: Hybrid (Ray)-

(Floquet Mode)-(MOM) algorithm and its GTD interpretation," *IEEE Trans. Antennas Propagat.*, Vol. 41, 412–421, 1993.

10. Felsen, L. B. and L. Carin, "Diffraction theory and of frequency- and time-domain scattering by weakly aperiodic truncated thin-wire gratings," *J. Opt. Soc. Am. A*, Vol. 11, 1291–1306, 1994.
11. Capolino, F. and L. B. Felsen, "Frequency- and time-domain Green's function for a phased semi-infinite periodic line array of dipoles," *IEEE Trans. Antennas Propagat.*, Vol. 50, 31–41, 2002.
12. Carin, L., L. B. Felsen, and T.-T. Hsu, "High-frequency fields excited by truncated arrays of nonuniformly distributed filamentary scatterers on an infinite dielectric slab: Parameterizing (leaky mode)-(Floquet mode) interaction," *IEEE Trans. Antennas Propagat.*, Vol. 44, 1–11, 1996.
13. Papoulis, A., *The Fourier Integral and Its Applications*, McGraw-Hill, New York, NY, 1962.
14. Felsen, L. B. and N. Marcuvitz, *Radiation and Scattering of Waves*, Prentice-Hall, Englewood Cliffs, NJ, 1973.
15. Abramowitz, M. and I. A. Stegun, *Handbook of Mathematical Functions*, Dover, New York, NY, 1964.
16. Guglielmi, M. and D. R. Jackson, "Low-frequency location of the leaky-wave poles for a dielectric layer," *IEEE Trans. Microwave Theory Tech.*, Vol. 38, 1743–1746, 1990.
17. Mahmoud, S. F. and A. J. Viitanen, "Surface wave character on a slab of metamaterial with negative permittivity and permeability," *Progress In Electromagnetics Research*, PIER 51, 127–137, 2005.
18. Li, C., Q. Sui, and F. Li, "Complex guided wave solution of grounded dielectric slab made of metamaterials," *Progress In Electromagnetics Research*, PIER 51, 187–195, 2006.
19. Kusaykin, O. P., P. N. Melezhik, A. Y. Poyedynchuk, and O. S. Troschylo, "Absorbing properties of a negative permittivity layer placed on a reflecting grating," *Progress In Electromagnetics Research*, PIER 64, 135–148, 2006.
20. Yang, R., Y. Xie, P. Wang, and L. Li, "Microstrip antennas with left-handed materials substrates," *J. Electromagn. Waves Appl.*, Vol. 20, 1221–1233, 2006.